Organic Electronics 60 (2018) 1–8

Contents lists available at ScienceDirect

Organic Electronics

journal homepage: www.elsevier.com/locate/orgel

Plasmonic enhancement for high efficient and stable perovskite solar cells by employing "hot spots" Au nanobipyramids

Hua Dong[a,b], Ting Lei[a], Fang Yuan[a], Jie Xu[a], Yong Niu[a], Bo Jiao[a], Zhenxi Zhang[b], Dawei Ding[d], Xun Hou[a], Zhaoxin Wu[a,c,*]

[a] Key Laboratory of Photonics Technology for Information, Key Laboratory for Physical Electronics and Devices of the Ministry of Education, School of Electronic and Information Engineering, Xi'an Jiaotong University, Xi'an, 710049, China
[b] Department of Biomedical Engineering, School of Life Science and Technology, Xi'an Jiaotong University, Xi'an, 710049, China
[c] Collaborative Innovation Center of Extreme Optics, Shanxi University, Taiyuan, 030006, China
[d] Department of Chemistry, School of Science, Xi'an Jiaotong University, Xi'an, 710049, China

ARTICLE INFO

Keywords:
Perovskite solar cells
Plasmonic effect
Hot spots
Trap density of states
Stability

ABSTRACT

Metal plasmonic effect is one promising way for improving the performance and stability of the perovskite solar cells via optical-electrical behalves, and the ability is in proportion to the enhanced local electromagnetic fields induced by metal nanostructures. In our work, unique gold nanobipyramids (Au NBs) structures were explored and incorporated in the hole transport layer of planar heterojunction PSCs. This typical "bipyramid-like" metal nanostructure with sharp tips has the multiple and strong plasmonic absorption properties from visible to the NIR, exhibiting high plasmonic-induced probability. In addition, generated "hot spots" around Au NBs provided much stronger EM fields enhancements than conventional Au nanoparticles, hence enhanced light harvesting and improved interfacial charge dynamic process can be achieved simultaneously. As for the further investigation of the electrical property, hot holes injection induced by Au NBs effectively filled in the interfacial traps under operation condition, contributing to the improvement of the open circuit voltage, the elimination of the hysteresis effect and the long-term stability. Accordingly, the best PSC incorporated with Au NBs showed the PCE of 18.84% whereas the reference device just showed the PCE of 16.02%. Our work demonstrated that plasmonic metal nanostructures possessing the feature of "hot spots" offered a great potential to further expand the performance limitation and operation tolerance of the PSCs.

1. Introduction

Metal halide perovskite materials have attracted much attention due to the advantages of tunable band energy, high absorption coefficient and long carriers diffusion length [1–4]. The power conversion efficiencies of perovskite solar cells (PSCs) undergoes a rapid development from 3.8% to 22.7% within a few years and have potential to be further increased [5,6]. Although multidisciplinary efforts have led to the rapid increase of the PCE to the level of silicon/CIGS solar cells, further improvements of PSCs performance and stability are still necessary for accelerating the commercialization. To date, substantial strategies, including the design of the organic/inorganic perovskite materials with different components, synthesis of new transporting layers and the interfacial-modification engineering, have been devoted to breaking through the limitation of performance [7–12]. Nonetheless, considering that both the light-harvesting and charge dynamic processes are the key points influencing the performance of the PSCs, it is more meaningful to develop the technology with dual optical-electrical tunable effects.

Plasmonic metal nanoparticles are nanoobjects with fascinating properties, making them a subject of great interest regarding the field of optoelectronics [13–18], especially the successful applications as an effective optical-electronic engineering tool in PSCs [19–22]. The localized surface plasmon resonance (LSPR) effect can be excited from the light-induced collective oscillation of their conduction band electrons on the surface of metal nanostructures, which result in the local electromagnetic fields (EM fields) enhancement around metal surfaces [23]. By adjusting of the materials, size, shape, and surrounding medium of the nanostructures, it could achieve the effective control of the range of the LSPR and the intensity of the local EM fields [24]. The LSPR of spherical nanoparticles is essentially located in the visible wavelength with single plasmonic peak. While anisotropic architectures are extremely interesting since they present different frequencies of resonance

* Corresponding author. Key Laboratory of Photonics Technology for Information, Key Laboratory for Physical Electronics and Devices of the Ministry of Education, School of Electronic and Information Engineering, Xi'an Jiaotong University, Xi'an, 710049, China.
E-mail address: ZhaoxinWu@mail.xjtu.edu.cn (Z. Wu).

https://doi.org/10.1016/j.orgel.2018.05.030
Received 1 May 2018; Received in revised form 14 May 2018; Accepted 20 May 2018
Available online 22 May 2018
1566-1199/

with a broadband absorption (from visible to NIR) depending on the polarization (longitudinal, transverse), which expand the scale of applications [25,26].

As for the optical aspect, plasmonic effect could enhance the light coupling and scattering into the active layer of PSCs. Au@TiO_2 nanorods, Au@SiO_2 nanorods and Au nanostars have been successfully applied to the PSCs, showing the efficient broadband absorption enhancement [19,22,27]. When it comes to the electronic aspect, it is generally attributed to the reduced exciton binding energy and the promotion of carrier transport and collection [21,28].

In spite of constantly processing the studies on the plasmonic enhanced effect for PSCs, the ultimate principle, specifically on interfacial charge dynamic process, should be identified and further addressed in plasmonic PSCs. Furthermore, whether in optical feature or in electrical feature, excellent ability of the EM field enhancement via metal nanostructures is crucially required in plasmonic PSCs research. Thus the exploration of typical metal geometry with much stronger EM field factor is extremely rewarding.

In regard to the plasmonic field, unique “hot spots” effect, which means the much drastically intensified EM field, could be generated at the corners of sharp features on metal nanoparticles by taking advantage of the “lightning rod” effect [29,30]. For the anisotropic geometries, sharp structures such as nanocubes, nanorices and nanobipyramids have proven to be very interesting since the EM field around their tips is much stronger compared to saponaceous nanorods with same specifications [31–33]. Considering this, development of the typical plasmonic nanostructures is the preferable choice of further improving the performance of the PSCs through the adjustment of the dual optical-electronic properties.

In this article, unique Au nanobipyramids (Au NBs) structures are explored and embedded in the hole transport layer (HTL) of planar heterojunction PSCs. This “pyramid-like" metal nanostructure has the wide and strong plasmonic absorption properties with the region from visible to the near-infrared, thus the Plasmon Resonance can be excited more effectively by avoiding the light trapping competition with the perovskite active layer. Besides the well-known contribution of enhanced light harvesting, the modulation of the electrical properties by Au NBs is more attractive in plasmonic PSCs, which is assumed as the main role of the improvement of the device performance. Under the excited state, unique “hot spots” characteristic could induce more intense EM field enhancements around the corners of Au NBs than conventional Au nanoparticles, which could significantly facilitate the exciton dissociation, charges transportation at the interface of PSCs. More importantly, owing to the hot holes injection effect by Au NBs under illumination, interfacial traps of the PSCs can be effectively filled, suppressing the charge recombination and shifting the quasi-Fermi energy level at the HTL/perovskite interface. Benefiting from these advantages, PSCs incorporated with optimal concentration of Au NBs show the typical PCE of 18.05% whereas the reference device just showed the typical PCE of 15.01%, accompanying with the improvement of the open circle voltage and the excellent tolerance of ambient air and operation. We think that plasmonic metal nanostructures with the advantage of “hot spots” feature could offer a great potential to further break the performance limitation of the PSCs as well as maintain the long-term operational stability.

2. Results and discussion

2.1. Characterization of Au NBs

The synthesis of nano-bipyramids was achieved via the seed-mediated growth approach [34]. Fig. 1a showed the SEM images of the Au NBs, and Fig. 1b and c showed the TEM image of the Au NBs. It can be seen that the bipyramids show regular diamond-like shapes with straight edges. The average length and diameter of bipyramids were 45–50 nm and 15–18 nm respectively, with aspect ratios between 3 and 3.3. EDX spectrum was also used to confirm the content of the Au NBs, and the Au peaks were clearly observed (shown in Fig. S1 and Table S1).

In fact, the plasmon wavelengths of the anisotropic metal architectures can be regulated from the visible to near-infrared regions by varying shape and aspect ratio of the nanostructures. Fig. 1d showed the absorption spectrum of the Au NBs, with two strong plasmonic peaks, attributed to the longitudinal and the transverse plasmonic absorption. The longitudinal and transverse plasmon resonance wavelengths of the initial Au NBs sample dispersed in aqueous solutions were 806 and 521 nm, respectively. Considering that the absorption edge of conventional $CH_3NH_3PbI_3$ was around 800 nm (shown in Fig. 1d), such an elaborate design avoided the competition with the perovskite layers as well as promise the extra light-trapping in low energy region (wavelength > 700 nm).

In addition to the wide absorption feature of the Au NBs, another unique characteristic of the Au NBs, was the “hot spots” property, which was emphasized in our study. Researches showed that “hot spots” can be generated at the tip of a sharp feature on a nanoparticle by taking advantage of the “lightning rod effect” [30,35]. The attractively induced dipoles were more easily formed on the corners and tip of the geometry, leading to the increased polarization vector density. Thus the drastically intensified EM field can be achieved around the sharp nanostructures, which was much larger than that of conventional metal nanostructures [36,37]. In fact, for the application of the plasmonic optoelectronic devices, the enhanced EM factor of the metal nanostructures was closely related to the improved performance of the devices, hence the typical metal nanostructures with strong intensified EM field has the huge potential to contribute to the plasmonic devices.

To gain a better understanding of the relationship between EM-field enhancement and the architecture of the metal nanostructures, We performed simulations for three structures with similar specifications: Au nanospheres (diameter ~20 nm), Au nanorods (same dimension as Au NBs) and Au NBs. A theoretical investigation (finite difference time-domain method: FDTD) on was utilized to calculate the distributions of E-field enhancement. Fig. 2 showed the simulation results of the field intensity enhancements of the Au NBs, Au NRs and Au NPs, respectively. The field intensity enhancements were calculated under the excitation at their plasmon wavelengths. The largest EM field enhancement appeared on the Au NBs and highly localized at the corner sites (Fig. 2a and b). Nevertheless, although the EM fields were enhanced on Au NRs and Au NPs, there was no hot spots formed.

The maximum fields intensity enhancement factors along the central length axis were plotted in Fig. 2f. The maximum enhancement factors of the Au NBs, Au NRs and Au NPs were 127(at 524 nm), 46(at 521 nm) and 15(at 535 nm), respectively. The simulation confirmed the superior EM fields enhancement effect of the Au NBs compared with the other nanoparticles without “hot sports” feature, which was crucial for plasmonic enhanced PSCs. For the experimental comparison, Au NPs and Au NRs were also synthesized, and the TEM images and absorption spectrum were shown in Fig. S2. Under the same concentration, Au NBs exhibited the stronger absorption intensity and sharper plasmonic peak than Au NRs and Au NPs, which was corresponding with the theoretical calculation.

2.2. PSCs with "hot spots" Au NBs

2.2.1. Optical and material properties of the films

For the applications of the Au NBs in PSCs, an inverted planar heterojunction structure (ITO/PSS:PEDOT/VO_x/$CH_3NH_3PbI_3$/$PC_{61}BM$/BCP/Ag) was designed, and the schematic of plasmonic PSCs was shown in Fig. 3a. Here such a multi-layer PSS:PEDOT/VO_x hole transporting layer (HTL) could effectively promote the charge transporting due to the excellent conductivity and appropriate energy level alignment [38,39]. Meanwhile, inorganic VO_x layer prevent the invasion of the moisture and oxygen. For the study of the plasmonic enhancement,

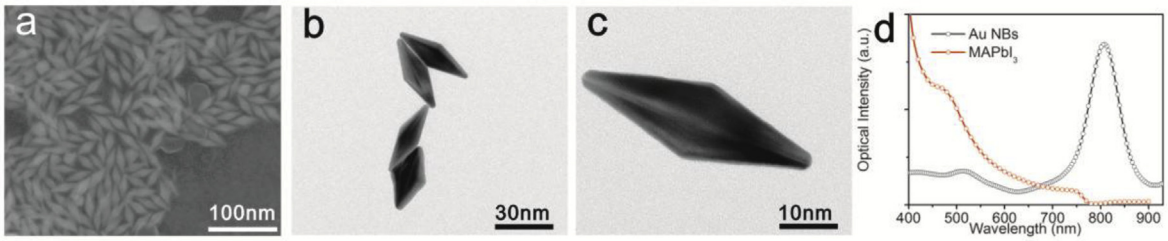

Fig. 1. (a) SEM images of the Au NBs. **(b,c)** TEM images of the Au NBs. **(d)** Absorption spectrum of the Au NBs and perovskite film.

Au NBs was buried into the VO_X layer to avoid the direct connection with the active layer, cause the charge quenching will take place via a nonradiative energy transfer process at the surfaces of metal nanostructure.

The SEM and AFM images of different $CH_3NH_3PbI_3$ films were shown in Fig. 3b–e and Fig. S3. It was found that surface morphology of two films have almost no apparent morphological differences, which was both continuous and compact. Actually, consider that the multiple HTL could effectively cover the Au NBs, the growth and the crystallization process of the perovskite film was just influenced by the surface properties of the VO_X. Fig. 3f exhibit the XRD patterns of $CH_3NH_3PbI_3$ thin films deposited on the HTL layer with and without Au NBs. The main diffraction peaks at the 2θ angles of 14.1° and 28.7°, can be assigned to (110) and (220) crystal faces of $CH_3NH_3PbI_3$ polycrystal, respectively [40]. Here two kinds of $CH_3NH_3PbI_3$ films showed very similar diffraction peaks as well as the peak intensity, suggesting the similar crystalline characteristic.

2.2.2. *J-V curves characteristics*

To investigate the advantages of Au NBs systematically, a bunch of

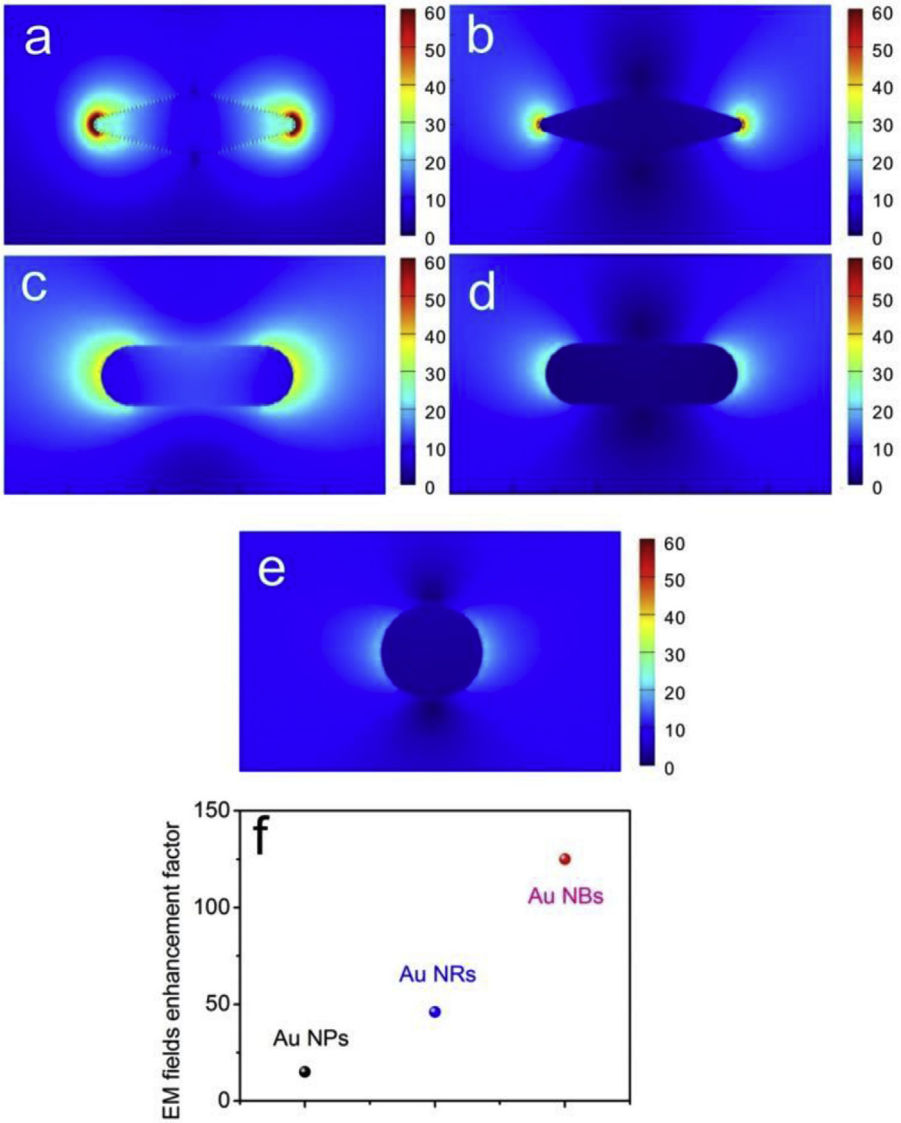

Fig. 2. The calculated distribution of localized electric field intensity around different metal nanostructures at their plasmonic resonance wavelengths: (a) 521 nm and (b) 806 nm for Au NBs. (c) 524 nm and (d) 804 nm for Au NRs. (e) 535 nm for Au NPs. (f) The maximum EM-field enhanced factor of three nanostructures.

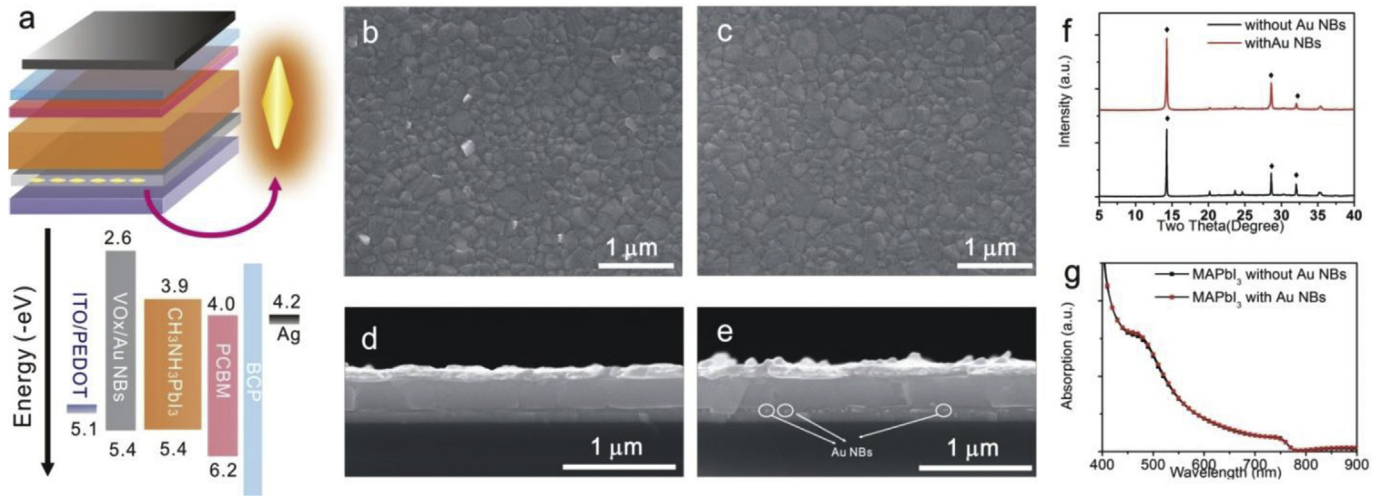

Fig. 3. (a) Schematic structure of P-I-N planar heterojunction perovskite solar cells (PSCs) incorporated with Au NBs in HTL. (b) top-view and (d) cross-section SEM images of reference PSC. (c) top-view and (e) cross-section SEM images of PSC with Au NBs. (f) XRD patterns and (g) Absorption spectrum of perovskite films with/without Au NBs.

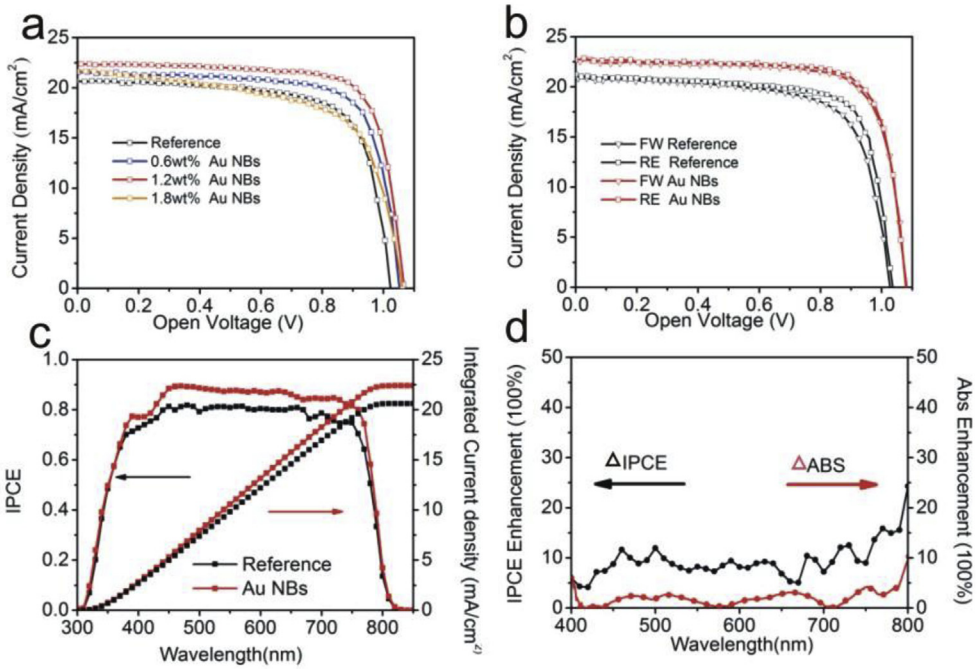

Fig. 4. (a) J-V curves of the devices incorporated with different concentrations of Au NBs. (b) J–V curve of the optimized devices with/without Au NBs, under reverse and forward scans. (c) IPCE results and integrated current density of devices with/without Au NBs. (d) Calculated wavelength-dependent enhancement factors of the IPCE (ΔIPCE) and absorption (ΔAbs) of devices with/without Au NBs.

solar cells was prepared with a series of concentrations condition (0.0 wt%, 0.6 wt%, 1.2 wt%, 1.8 wt%). Here the typical J-V characteristics and statistical analysis of the photovoltaic parameters of devices were shown in Fig. 4a and Fig. S4, respectively. Compared to the reference device without Au NBs, the performance of the devices incorporated with Au NBs exhibit an increase-to-decrease tendency with the increase of the concentrations, and the optimized concentration was 1.2 wt%. For the concentration less than optimum, a rather low distribution of Au NBs just contributed slight plasmonic effects; while the excessive concentration was also adverse to the device performance cause those extra plasmonic particles might serve as traps for photogenerated carriers and lead to the increased interfacial roughness. For the optimized concentration, the typical parameters of the device with Au NBs was J_{sc} of 22.31 mA/cm^2, V_{oc} of 1.064 V, FF of 76.1% and PCE of 18.05%, which showed a dramatically enhancement compared with reference device (J_{sc} of 20.44 mA/cm^2, V_{oc} of 1.024 V, FF of 71.3% and PCE of 15.01%) due to the enhanced V_{oc}, J_{sc} and FF. The aforementioned results suggested that the introduction of the Au NBs with appropriate distribution could dramatically improve the performance of PHJ-PSCs. For the horizontal comparison of the plasmonic enhancement with different nanostructures, Au NRs and Au NPs were also synthesized and employed in PSCs, and the performance parameters of the devices with different Au nanostructures were shown in Fig. S5 and Table S2-4. For the device with optimal concentration of the Au NPs, the parameters of the typical performance is J_{sc} of 21.88 mA/cm^2, V_{oc} of 1.041 V, FF of 74.3% and PCE of 16.92%; Au NRs show a little excellent enhanced than Au NPs, with the performance (J_{sc} of 22.13 mA/cm^2, V_{oc} of 1.052 V, FF of 74.7% and PCE of 17.39%). However, the increase of each parameter was limited, especially for the Voc and FF. Considering that V_{oc} and FF were mainly determined by the electrical properties of PSCs [19,41], the better performance of the Au NBs should be attributed to the more intense EM filed than that of the Au NRs and Au NPs.

More attractively, the PHJ-PSC device with Au NBs showed less

hysteresis than the reference devices, prospected to delay the degradation of the perovskite semiconductors. Based on the optimized concentration, a champion PHJ-PSC device was achieved with the PCE of 18.84%(18.68%) under reverse (forward) scanning, of which the V_{oc}, J_{sc}, FF are 1.078 V (1.077 V), 22.68 mA/cm^2 (22.64 mA/cm^2), 77.1% (76.0%) respectively, as shown in Fig. 4b. The negligible hysteresis was supposed as the effect of interfacial trap passivation [42,43], leading to the restrained ion migration and more balanced charge mobility.

It was known that the performance improvement of plasmonic PSCs was the cooperation of both optical and electrical behaviors. To investigate the different proportions of the contribution, the IPCE spectra and integrated current density of best PSCs incorporated with/without Au NBs were measured and shown in Fig. 4c. It indicated that significant enhancement in IPCE took place over almost the whole wavelength range, and the related enhancement of the IPCE (ΔIPCE) and absorption (ΔABS) was calculated and plotted in Fig. 4d. It was found that was the enhancement of the IPCE was obvious compared to the negligible change of the absorption. Meanwhile, the variation tendency of ΔIPCE was no-wavelength selectivity, inconsistent with that of ΔABS. The comparison result showed that the slight incorporation of Au NBs with the device just developed little gain of the absorption. Although extra trapped light in the neighboring area of Au NBs would be beneficial for the generation of more charges, the light-harvesting contribution of the Au NBs may still play a minor role of improving the performance of PSCs, expressed as the partial effect of the improved J_{sc}. Correspondingly, the electrical behaviors of the Au NBs would play a major role of the enhancement of the PSC devices performance, which was responsible for the increase parameters (V_{oc}, FF and partial J_{sc}) in plasmonic modified PSCs.

2.2.3. Charge dynamic modification and stability of plasmonic PSCs

The PCE evolution of PSCs with different Au nanostructures showed that Au NBs with “hot spots” exhibit the best performance. Benefiting from the unique “hot spots” effect, much stronger intensity of the EM field around the Au NBs can be obtained compared to conventional Au nanoparticles. In terms of this, it was expected that Au NBs could offer the superior electrical modification ability for the PSCs. A series of approaches related to charge dynamic process, including time-resolved photoluminescence (TRPL) measurements, Electrochemical Impedance Spectroscopy (EIS), charge injection current measurement, analysis of the traps of density (tDOS) and the measurement of the Mott-Schottky, were developed to further investigate the possible factors contributing to the performance improvement.

Considering the doping position of the Au nanostructures in our experiment, one electrical behavior was generally expressed as the facilitation of charge separation and the inhibition of the charge recombination at the metal-semiconductor interface [21,44]. TRPL measurements of the perovskite films on different HTL layers (HTL1:reference; HTL2: with Au NRs; HTL3: with Au NBs) and the glass substrate were shown in Fig. 5a. Compared to the reference perovskite/HTL structure, obvious quenching effect can be observed on both of the Au NRs/Au NBs structures. The PL lifetime of the perovskite/HTL1 was 13.35 ns, and that of the perovskite/HTL2 and perovskite/HTL3 were 11.98 ns and 10.02 ns respectively. whereas the lifetime of perovskite on glass substrate was 75.4 ns. The decrease of the PL lifetime in modified PSCs indicated the facilitated charge extraction process, and the assistance of Au NBs was more excellent than Au NRs.

To identify the influence of the plasmonic effect on recombination pathways in the PSCs, We continued to measure the EIS of devices under working conditions. Fig. 5d showed the Nyquist equivalent model, which was used to fit the parameters of the EIS data (Fig. S6). Here bulk and interface recombination were discussed separately to illustrate the whole charge recombination characteristics of the PSCs [45]. The surface charge recombination lifetime ($\tau_{surface}$) and bulk charge recombination lifetime (τ_{bulk}) with different bis-voltage were extracted from the EIS results and shown in Fig. 5b and c. The much longer τ_{bulk} mean the much slower recombination process, which was assumed to the excellent quality of the perovskite films with a low density of bulk defects. Considering this, the surface charge recombination lead to the main pathways in the PSCs.

For three types of PSCs, the difference of the τ_{bulk} under the same bis-voltage was very small. Whereas, the $\tau_{surface}$ of two plasmonic PSCs exhibit an obvious increase compared that of ref PSCs, and PSCs with Au NBs show the largest value of $\tau_{surface}$ under each voltage. The analysis of the EIS declared that the introduction of the Au NBs could sufficiently suppress the surface recombination while having little influence on the bulk recombination. Here the suppression the surface recombination was express as the interfacial modification at HTL/perovskite interface. Actually, as the major detrimental of the electrical behaviors in PSCs, the interface recombination of the PSCs was closely linked to the interface trap density of states [45]. In terms of this, the exploration of the t-DOS variation influenced by Au nanostructure in plasmonic PSCs was of great importance.

Thermal admittance spectroscopy (TAS) was a well-established, effective technique for characterizing both shallow and deep defects, which has been broadly applied in understanding defects in solar cells [46,47]. In our study, TAS method was utilized and the result was shown in Fig. 6a. The energetic profile of trap density of states (tDOS) can be derived from the angular frequency dependent capacitance (shown in supplement information). As for the reference device, trap density distributed from 2.9×10^{16} m^{-3} to 9.7×10^{18} m^{-3}, and a decreased tendency of tDOS was observed in the device with Au NRs, showing the effective passivation of charge traps. For the device with Au NBs, the distribution of tDOS was lowest, especially in the relatively deep trap states by 1–2 order of magnitudes (> 0.25eV). In view of the location of the Au NBs incorporated in PSCs, the formation of charge trapping sites was prevented at HTL/perovskite interface, which was in good accordance to our assumption from the EIS measurement.

In our study, another interesting phenomenon was obvious V_{oc} enhancement observed in plasmonic modified PSCs, in particular of employing Au NBs. For the planar p-i-n heterojunction solar cells, the V_{oc} was primarily related to the built-in potential (V_{bi}) [48]. Here the built-in potential $e{\cdot}V_{bi}$ was defined as the split of quasi-Fermi energy levels between the p-type HTL (E_{Fp}) and n-type ETL (E_{Fn}) in the optoelectronic devices [49]. By utilizing the capacitance-voltage measurement, the Mott-Schottky curves of PSCs with/without Au NBs was derived and shown in Fig. 6b [50]. The V_{bi} of the reference devices with Au NRs and Au NBs were 1.015 V and 1.041 V, respectively. Considering the metal nanostructures buried in the HTL, the origin of the improved V_{bi} was assumed as the shift down of the E_{Fp} at the HTL/Perovskite interface.

In semiconductors, the distribution of the trap density of states could influence the position of the quasi-Fermi energy level (E_F), and the shift of the E_F would occur when the trap states were filled in [51]. In fact, the induced plasmonic hot carrier generation process, which was one of the most significant characteristics in metal plasmonic fields, provided the possibility for trap filling.

Under illuminating, plasmonic hot carriers generation of the metal nanoparticles in the semiconductor can be excited due to the decay of surface plasmon in the metal-dielectric interfaces, and hot holes generation dominated in p-type semiconductor while hot electrons generation occurred in n-type semiconductor. Thus the plasmon-induced charge injection across the Schottky barrier could achieve the trap passivation in VO_x matrix and VO_x/perovskite interface. The proposed mechanism diagram of hot carrier injection process was depicted in Fig. 6d. Owing to the decay of plasmon, photons with matching frequency can be captured by Au NBs via surface plasmon resonance, then energetic electron-hole pairs in the s-band were generated subsequently [52]. Hot electrons generated in this process cannot reach such a higher conductive band (CB) of VO_x, but has the possibility of injecting to the LUMO of $MAPbI_3$ due to favorable energy level alignment, corresponding the hot hole generated from in this process could easily transferable to the valence band (VB) of VOx. Such a hot charge

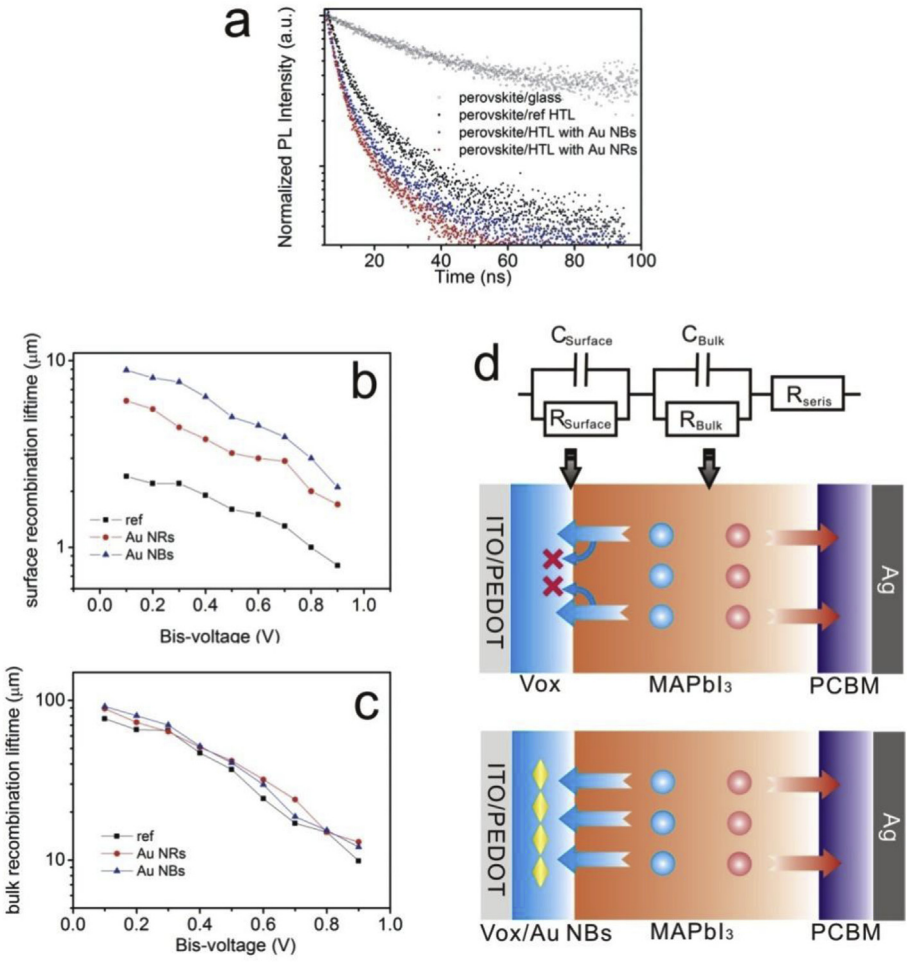

Fig. 5. (a) PL lifetime of the perovskite films on glass and different HTL. (b) surface recombination time and (c) bulk recombination time of different devices fitted from EIS. (d) Nyquist equivalent model and schematic of the recombination process in reference and plasmonic devices.

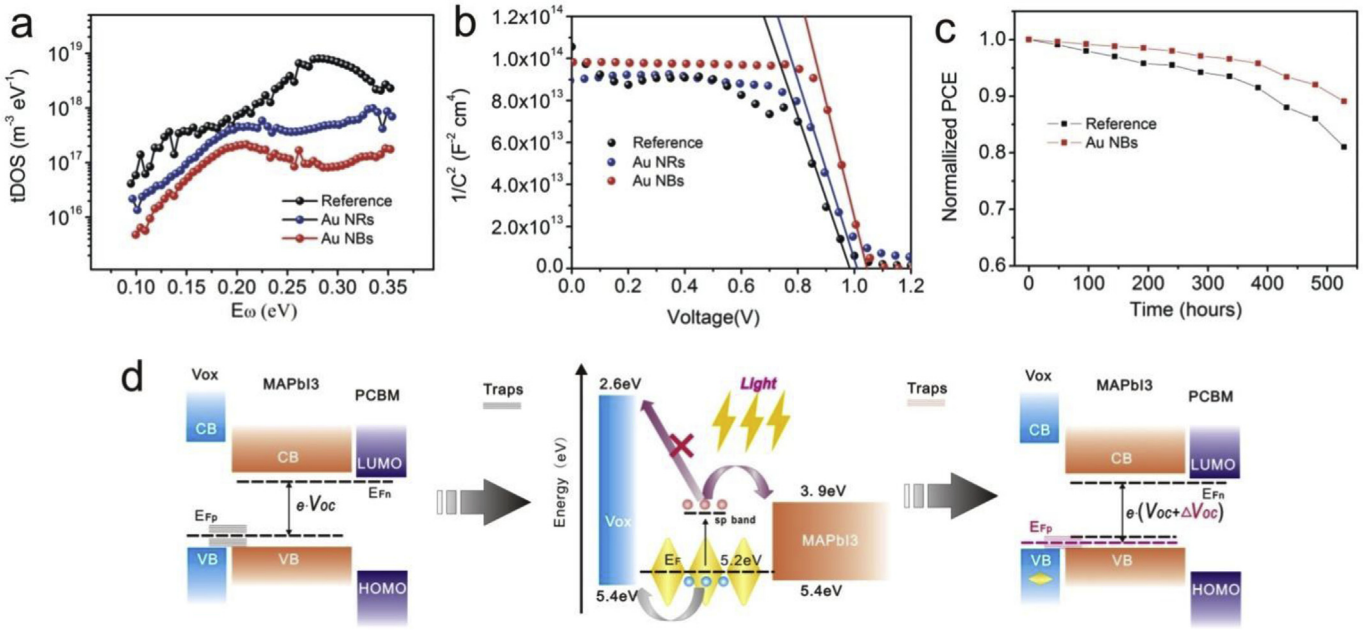

Fig. 6. (a) Trap density of states (tDOS) and (b) Mott-Schottky curves of the various devices (reference, with Au NRs, with Au NBs). (c) Efficiency evolution of the devices with/without Au NBs under 1 sun illumination. (d) Mechanism schematic diagram of hot hole injection process for the trap-filling and related enlarged built-in potential of the device due to the shift of the quasi-Fermi level of the perovskite/HTL.

injection process could result in the effective trap healing effect at the HTL/Perovskite interface.

Beyond the trap healing effect by hot holes injection process, the conductivity of the modified HTL was improved as well. Here the J-V curves of HTL with/without Au NBs were measured under dark/illustration conditions and shown in Fig. S7. Under dark condition, the slight enhancement of the conductivity can be attributed to the excellent conductor property of the Au NBs. While under illumination condition, the slope of the J-V curve measured by HTL with Au NBs was obviously larger than that of the HTL without Au NBs. The much higher photoconductivity of the modified HTL means the reduced series resistance of the device, which has a positive impact on the improved charge extraction and voltage of the devices.

Benefiting from the restriction of the charge traps induced by Au NBs, the shortcomings of interfacial reactions and the ion migration in PSCs can be improved, thereby eliminating notorious photocurrent hysteresis and prolonging operational stability [53]. PSCs with/without Au NBs were stored in ambient air without encapsulation (room temperature and humidity ~50%), and the device performance was measured periodically (constantly working 2 h for every 2 days). Thus the efficiency evolution of the PSCs was the combined consequence of both moisture resistance and the operational stability. For the reference device, the inorganic VO_x layer could effectively block the invasion of the oxygen and moisture, still retaining 81.5% of its original efficiency after 500 h. As a comparison, the device with Au NBs has an even better durability, which just suffered 8% efficiency loss. The suppression of trap filling by utilizing hot hole injection through metal NPs could contribute to the reduction of the hysteresis effect, also supposed as a promising route for the extension of the PSC lifetime.

3. Conclusions

In summary, unique gold nanobipyramids (Au NBs) nanostructures were utilized to and incorporate into the hole transport layer of planar heterojunction PSCs. This typical “bipyramid-like" metal nanostructure has the multiple and wide plasmonic absorption, with the efficient plasmon excitation probability, hence both the enhanced light harvesting and improved electrical properties can be achieved. In addition, due to the “hot spots” around sharp Au NBs, much stronger EM fields enhancements can be excited than conventional Au nanoparticles, especially providing more advantages of electrical benefit. The induced Hot holes injection induced by Au NBs could heal charge traps at the HTL/perovskite interface, contributing to the improvement of the open circuit voltage, the elimination of the hysteresis effect and the operational stability. At last, the optimized device with Au NBs shows a considerable performance enhancement from 16.02% to 18.84%. Our results demonstrated that plasmonic metal nanostructures possessing the feature of “hot spots” opens the way for further improving the efficiency, electrical characteristics and stability of PSCs.

4. Experimental section

4.1. Materials and pre-formed perovskite film preparation

PbI_2 (99.999 wt%) was purchased from Alfa Aesar and used as received. Vanadium triisopropoxy oxide (96%) was purchased from Alfa Aesar and diluted before using. $PC_{61}BM$ (99.5%) was purchased from Solenne and used as received. BCP was purchased from Nichem. CH_3NH_3I was synthesized by reacting 33 wt% CH_3NH_2 in ethanol with 57% HI in water solution at a 2:1 M ratio of CH_3NH_2 to HI and 0 °C for 2 h. The precipitate of CH_3NH_3I was gained by rotary evaporation at 40 °C and washed with dry diethyl ether until the solid became white. The final product was dried at 60 °C in a vacuum oven for 24 h. The Au nanobipyramids, Au nanorods and Au nanospheres were synthesized by the seed-mediated growth method [34,54].

4.2. Device completion

ITO-coated glass (20 square^{-1}) substrates were sequentially cleaned with detergent, deionized water, acetone for 15 min before drying. After drying under a N_2 stream, substrates were further cleaned by a UV ozone treatment for 5 min.

PSS:PEDOT(AL4083, volume ratio of 1:3 in deionized water) was spin-coated onto the ITO substrates as the buffer layer at 3000 rpm for 30 s, and the samples were then annealed at 150 °C for 20min.

For controlled inorganic VO_x HTL layer: Vanadium triisopropoxy oxide was diluted by deionized water with the volume ratio of 1:50 as the VO_x precursor, and Au NBs/Au NRs or Au NPs were added into the VO_x precursor with a series of concentrations. The initial and modified precursor was spin-coated onto PSS:PEDOT films at 2000 rpm for 30 s, subsequently annealed at 120 °C for 30min.

The perovskite precursor solution was made by dissolving an equimolar ratio of PbI_2 (1.2 M)and CH_3NH_3I (1.2 M) into a mixed solvent of DMF and DMSO (volume ratio of 8:2) at 60 °C. Perovskite layers were formed by spin-coating the precursor solution at 5000 rpm for 35 s. At the first 10 s, the substrate was treated with toluene drop-casting (0.8 mL). The resulting perovskite films were annealed at 60 °C for 1 min and 100 °C for 10 min. 20 mg mL^{-1} $PC_{61}BM$ in chlorobenzene was then spin-coated on perovskite film at 2000 rpm respectively for 30 s 6 nm BCP and 120 nm Ag were thermally evaporated onto the PCBM layer to eventually consummate the device.

4.3. Material and device characterization

A field emission scanning electron microscope (SEM) (Quanta 250, FEI, USA) was used to investigate the morphology and crystallinity. The crystalline structure on ITO substrate was performed by a X-ray diffractometer (Bruker D8 ADVANCE) with Cu Kα radiation. The absorption spectra were obtained by UV-Vis spectrophotometer (HITACHI U-3010, Japan). The time-resolved PL spectra were recorded by a 100 ps time resolution using a time-correlated single photon counting (TCSPC) system (FLS920 spectrometer) (excited by picosecond pulsed LEDs, pulse duration: < 850 ps, repetition rate: 10 MHz). The photovoltaic performance was estimated under an AAA solar simulator (XES-301S, SAN-EI), AM 1.5G irradiation with an intensity of 100 mW cm^{-2}. The photocurrent-voltage (J-V) curve was measured by a Keithley (2602 Series Sourcemeter), and the scan rates were performed with a 0.2 V s^{-1} step. Incident photon-to-current conversion efficiency (IPCE) spectra were collected at AC mode by the solar cell quantum efficiency measurement system (SolarCellScan 100, Zolix instruments. Co. Ltd). The area of each device, calibrated by the shadow mask, was 9.00 mm^2. Electrochemical impedance spectroscopy (EIS) of the cells were evaluated using CHI-660E over the frequency range of 0.1 Hz–100 KHz under the illumination (100 mW cm^{-2}).

Acknowledgment

This work was financially supported by National Natural Science Foundation of China (Grant Nos. 11574248, 61604121). International Cooperation by Shaanxi (Grant No. 2015KW-008), China Postdoctoral Science Foundation (Grant No. 2016M590947) and the Fundamental Research Funds for the Central Universities(Grant No. xjj2016031). The SEM and TEM work was performed at International Center by Dielectric Research (ICDR), Xi'an Jiaotong University, Xi'an, China. The authors thank Mr. Ma/Miss Dai for his/her help in using SEM. We also thank Dr. Huang at Instrument Analysis Center of Xi'an Jiaotong University for their assistance with XRD analysis.

Appendix A. Supplementary data

Supplementary data related to this article can be found at http://dx.doi.org/10.1016/j.orgel.2018.05.030.

References

[1] W.Y. Nie, H.H. Tsai, R. Asadpour, J.C. Blancon, A.J. Neukirch, G. Gupta, J.J. Crochet, M. Chhowalla, S. Tretiak, M.A. Alam, H.L. Wang, A.D. Mohite, High-efficiency solution-processed perovskite solar cells with millimeter-scale grains, Science 347 (2015) 522–525.

[2] K.X. Steirer, P. Schulz, G. Teeter, V. Stevanovic, M. Yang, K. Zhu, J.J. Berry, Defect tolerance in methylammonium lead triiodide perovskite, Acs Energy Lett. 1 (2016) 360–366.

[3] N.K. Kumawat, M.N. Tripathi, U. Waghmare, D. Kabra, Structural, optical, and electronic properties of wide bandgap perovskites: experimental and theoretical investigations, J. Phys. Chem. A 120 (2016) 3917–3923.

[4] S.D. Stranks, G.E. Eperon, G. Grancini, C. Menelaou, M.J.P. Alcocer, T. Leijtens, L.M. Herz, A. Petrozza, H.J. Snaith, Electron-hole diffusion lengths exceeding 1 micrometer in an organometal trihalide perovskite absorber, Science 342 (2013) 341–344.

[5] A. Kojima, K. Teshima, Y. Shirai, T. Miyasaka, Organometal halide perovskites as visible-light sensitizers for photovoltaic cells, J. Am. Chem. Soc. 131 (2009) 6050-+.

[6] https://www.nrel.gov/pv/assets/images/effciency-chart.png(accessed:November 2017), National Renewable Energy Laboratory (NREL)2017.

[7] H.S. Kim, J.Y. Seo, N.G. Park, Material and device stability in perovskite solar cells, Chemsuschem 9 (2016) 2528–2540.

[8] D. Chen, H. Zhang, Y. Liu, J.H. Li, Graphene and its derivatives for the development of solar cells, photoelectrochemical, and photocatalytic applications, Energy Environ. Sci. 6 (2013) 1362–1387.

[9] J. Huang, Y. Yuan, Y. Shao, Y. Yan, Understanding the physical properties of hybrid perovskites for photovoltaic applications, Nat. Rev. Mater. 2 (2017).

[10] A. Fakharuddin, L. Schmidt-Mende, G. Garcia-Belmonte, R. Jose, I. Mora-Sero, Interfaces in perovskite solar cells, Adv. Energy Mater. 7 (2017).

[11] C.T. Zuo, D. Vak, D. Angmo, L.M. Ding, M. Gao, One-step roll-to-roll air processed high efficiency perovskite solar cells, Nanomater. Energy 46 (2018) 185–192.

[12] C.T. Zuo, H.J. Bolink, H.W. Han, J.S. Huang, D. Cahen, L.M. Ding, Advances in perovskite solar cells, Adv. Sci. 3 (2016).

[13] C. Petridis, K. Savva, E. Kymakis, E. Stratakis, Laser generated nanoparticles based photovoltaics, J. Colloid Interface Sci. 489 (2017) 28–37.

[14] E. Stratakis, E. Kymakis, Nanoparticle-based plasmonic organic photovoltaic devices, Mater. Today 16 (2013) 133–146.

[15] H.J. Chen, L. Shao, Q. Li, J.F. Wang, Gold nanorods and their plasmonic properties, Chem. Soc. Rev. 42 (2013) 2679–2724.

[16] H. Dong, Z.X. Wu, A. El-Shafei, B. Xia, J. Xi, S.Y. Ning, B. Jiao, X. Hou, Ag-encapsulated Au plasmonic nanorods for enhanced dye-sensitized solar cell performance, J. Mater. Chem. 3 (2015) 4659–4668.

[17] Y.H. Jang, Y.J. Jang, S. Kim, L.N. Quan, K. Chung, D.H. Kim, Plasmonic solar cells: from rational design to mechanism overview, Chem. Rev. 116 (2016) 14982–15034.

[18] Y.H. Jang, A. Rani, L.N. Quan, V. Adinolfi, P. Kanjanaboos, O. Ouellette, T. Son, Y.J. Jang, K. Chung, H. Kwon, D. Kim, D.H. Kim, E.H. Sargent, Graphene oxide shells on plasmonic nanostructures lead to high-performance photovoltaics: a model study based on dye-sensitized solar cells, Acs Energy Lett 2 (2017) 117–123.

[19] R.S. Wu, B.C. Yang, C.J. Zhang, Y.L. Huang, Y.X. Cui, P. Liu, C.H. Zhou, Y.Y. Hao, Y.L. Gao, J.L. Yang, Prominent efficiency enhancement in perovskite solar cells employing silica-coated gold nanorods, J. Phys. Chem. C 120 (2016) 6996–7004.

[20] M. Qian, M. Li, X.B. Shi, H. Ma, Z.K. Wang, L.S. Liao, Planar perovskite solar cells with 15.75% power conversion efficiency by cathode and anode interfacial modification, J. Mater. Chem. 3 (2015) 13533–13539.

[21] N. Aeineh, E.M. Barea, A. Behjat, N. Sharifi, I. Mora-Sero, Inorganic surface engineering to enhance perovskite solar cell efficiency, ACS Appl. Mater. Interfaces 9 (2017) 13181–13187.

[22] R.D. Fan, L.G. Wang, Y.H. Chen, G.H.J. Zheng, L. Li, Z.L. Li, H.P. Zhou, Tailored Au@TiO2 nanostructures for the plasmonic effect in planar perovskite solar cells, J. Mater. Chem. 5 (2017) 12034–12042.

[23] X.H. Huang, S. Neretina, M.A. El-Sayed, Gold nanorods: from synthesis and properties to biological and biomedical applications, Adv. Mater. 21 (2009) 4880–4910.

[24] K.L. Kelly, E. Coronado, L.L. Zhao, G.C. Schatz, The optical properties of metal nanoparticles: the influence of size, shape, and dielectric environment, J. Phys. Chem. B 107 (2003) 668–677.

[25] A.V. Whitney, J.W. Elam, S.L. Zou, A.V. Zinovev, P.C. Stair, G.C. Schatz, R.P. Van Duyne, Localized surface plasmon resonance nanosensor: a high-resolution distance-dependence study using atomic layer deposition, J. Phys. Chem. B 109 (2005) 20522–20528.

[26] C.J. Murphy, T.K. San, A.M. Gole, C.J. Orendorff, J.X. Gao, L. Gou, S.E. Hunyadi, T. Li, Anisotropic metal nanoparticles: synthesis, assembly, and optical applications, J. Phys. Chem. B 109 (2005) 13857–13870.

[27] R.T. Ginting, S. Kaur, D.K. Lim, J.M. Kim, J.H. Lee, S.H. Lee, J.W. Kang, Plasmonic effect of gold nanostars in highly efficient organic and perovskite solar cells, ACS Appl. Mater. Interfaces 9 (2017) 36111–36118.

[28] W. Zhang, M. Saliba, S.D. Stranks, Y. Sun, X. Shi, U. Wiesner, H.J. Snaith, Enhancement of perovskite-based solar cells employing core-shell metal nanoparticles, Nano Lett. 13 (2013) 4505–4510.

[29] P.S. Kumar, I. Pastoriza-Santos, B. Rodriguez-Gonzalez, F.J. Garcia de Abajo, L.M. Liz-Marzan, High-yield synthesis and optical response of gold nanostars, Nanotechnology 19 (2008).

[30] M. Rycenga, X.H. Xia, C.H. Moran, F. Zhou, D. Qin, Z.Y. Li, Y.A. Xia, Generation of hot spots with silver nanocubes for single-molecule detection by surface-enhanced Raman scattering, Angew. Chem. Int. Ed. 50 (2011) 5473–5477.

[31] F. Hao, C.L. Nehl, J.H. Hafner, P. Nordlander, Plasmon resonances of a gold nanostar, Nano Lett. 7 (2007) 729–732.

[32] E.C. Le Ru, J. Grand, I. Sow, W.R.C. Somerville, P.G. Etchegoin, M. Treguer-Delapierre, G. Charron, N. Felidj, G. Levi, J. Aubard, A scheme for detecting every single target molecule with surface-enhanced Raman spectroscopy, Nano Lett. 11 (2011) 5013–5019.

[33] H. Wei, A. Reyes-Coronado, P. Nordlander, J. Aizpurua, H.X. Xu, Multipolar plasmon resonances in individual Ag nanorice, ACS Nano 4 (2010) 2649–2654.

[34] D. Chateau, A. Liotta, F. Vadcard, J.R.G. Navarro, F. Chaput, J. Lerme, F. Lerouge, S. Parola, From gold nanobipyramids to nanojavelins for a precise tuning of the plasmon resonance to the infrared wavelengths: experimental and theoretical aspects, Nanoscale 7 (2015) 1934–1943.

[35] H. Wei, H.X. Xu, Hot spots in different metal nanostructures for plasmon-enhanced Raman spectroscopy, Nanoscale 5 (2013) 10794–10805.

[36] N.A. Hatab, C.H. Hsueh, A.L. Gaddis, S.T. Retterer, J.H. Li, G. Eres, Z.Y. Zhang, B.H. Gu, Free-standing optical gold bowtie nanoantenna with variable gap size for enhanced Raman spectroscopy, Nano Lett. 10 (2010) 4952–4955.

[37] K.D. Osberg, M. Rycenga, N. Harris, A.L. Schmucker, M.R. Langille, G.C. Schatz, C.A. Mirkin, Dispersible gold nanorod dimers with Sub-5 nm gaps as local amplifiers for surface-enhanced Raman scattering, Nano Lett. 12 (2012) 3828–3832.

[38] H.C. Sun, X.M. Hou, Q.L. Wei, H.W. Liu, K.C. Yang, W. Wang, Q.Y. An, Y.G. Rong, Low-temperature solution-processed p-type vanadium oxide for perovskite solar cells, Chem. Commun. 52 (2016) 8099–8102.

[39] H.T. Peng, W.H. Sun, Y.L. Li, S.Y. Ye, H.X. Rao, W.B. Yan, H.P. Zhou, Z.Q. Bian, C.H. Huang, Solution processed inorganic V2O (x) as interfacial function materials for inverted planar-heterojunction perovskite solar cells with enhanced efficiency, Nano Res. 9 (2016) 2960–2971.

[40] M.J. Carnie, C. Charbonneau, M.L. Davies, B. O'Regan, D.A. Worsley, T.M. Watson, Performance enhancement of solution processed perovskite solar cells incorporating functionalized silica nanoparticles, J. Mater. Chem. 2 (2014) 17077–17084.

[41] G. Kakavelakis, K. Petridis, E. Kymakis, Recent advances in plasmonic metal and rare-earth-element upconversion nanoparticle doped perovskite solar cells, J. Mater. Chem. 5 (2017) 21604–21624.

[42] S.K. Cushing, J.T. Li, J. Bright, B.T. Yost, P. Zheng, A.D. Bristow, N.Q. Wu, Controlling plasmon-induced resonance energy transfer and hot electron injection processes in Metal@TiO2 core-shell nanoparticles, J. Phys. Chem. C 119 (2015) 16239–16244.

[43] C. Clavero, Plasmon-induced hot-electron generation at nanoparticle/metal-oxide interfaces for photovoltaic and photocatalytic devices, Nat. Photon. 8 (2014) 95–103.

[44] J. Cui, C. Chen, J.B. Han, K. Cao, W.J. Zhang, Y. Shen, M.K. Wang, Surface plasmon resonance effect in inverted perovskite solar cells, Adv. Sci. 3 (2016).

[45] Y.H. Shao, Z.G. Xiao, C. Bi, Y.B. Yuan, J.S. Huang, Origin and elimination of photocurrent hysteresis by fullerene passivation in CH3NH3PbI3 planar heterojunction solar cells, Nat. Commun. 5 (2014).

[46] C. Melzer, E.J. Koop, V.D. Mihailetchi, P.W.M. Blom, Hole transport in poly(phenylene vinylene)/methanofullerene bulk-heterojunction solar cells, Adv. Funct. Mater. 14 (2004) 865–870.

[47] Z.G. Xiao, Q.F. Dong, C. Bi, Y.C. Shao, Y.B. Yuan, J.S. Huang, Solvent annealing of perovskite-induced crystal growth for photovoltaic-device efficiency enhancement, Adv. Mater. 26 (2014) 6503–6509.

[48] C. Uhrich, D. Wynands, S. Olthof, M.K. Riede, K. Leo, S. Sonntag, B. Maennig, M. Pfeiffer, Origin of open circuit voltage in planar and bulk heterojunction organic thin-film photovoltaics depending on doped transport layers, J. Appl. Phys. 104 (2008).

[49] I. Lange, J. Kniepert, P. Pingel, I. Dumsch, S. Allard, S. Janietz, U. Scherf, D. Neher, Correlation between the open circuit voltage and the energetics of organic bulk heterojunction solar cells, J. Phys. Chem. Lett. 4 (2013) 3865–3871.

[50] F. Fabregat-Santiago, G. Garcia-Belmonte, I. Mora-Sero, J. Bisquert, Characterization of nanostructured hybrid and organic solar cells by impedance spectroscopy, Phys. Chem. Chem. Phys. 13 (2011) 9083–9118.

[51] Y.C. Shao, Y.B. Yuan, J.S. Huang, Correlation of energy disorder and open-circuit voltage in hybrid perovskite solar cells, Nat. Energy 1 (2016).

[52] T. Barman, A.A. Hussain, B. Sharma, A.R. Pal, Plasmonic hot hole generation by interband transition in gold-polyaniline, Sci Rep-Uk 5 (2015).

[53] M. Sygletou, G. Kakavelakis, B. Paci, A. Generosi, E. Kymakis, E. Stratakis, Enhanced stability of aluminum nanoparticle-doped organic solar cells, ACS Appl. Mater. Interfaces 7 (2015) 17756–17764.

[54] B. Nikoobakht, M.A. El-Sayed, Preparation and growth mechanism of gold nanorods (NRs) using seed-mediated growth method, Chem. Mater. 15 (2003) 1957–1962.